Efficient Near-Infrared Electroluminescence at 840 nm with "Metal-Free" Small-Molecule:Polymer Blends

Alessandro Minotto, Petri Murto, Zewdneh Genene, Andrea Zampetti, Giuseppe Carnicella, Wendimagegn Mammo, Mats R. Andersson, Ergang Wang,* and Franco Cacialli*

Due to the so-called energy-gap law and aggregation quenching, the efficiency of organic light-emitting diodes (OLEDs) emitting above 800 nm is significantly lower than that of visible ones. Successful exploitation of triplet emission in phosphorescent materials containing heavy metals has been reported, with OLEDs achieving remarkable external quantum efficiencies (EQEs) up to 3.8% (peak wavelength > 800 nm). For OLEDs incorporating fluorescent materials free from heavy or toxic metals, however, we are not aware of any report of EQEs over 1% (again for emission peaking at wavelengths > 800 nm), even for devices leveraging thermally activated delayed fluorescence (TADF). Here, the development of polymer light-emitting diodes (PLEDs) peaking at 840 nm and exhibiting unprecedented EQEs (in excess of 1.15%) and turn-on voltages as low as 1.7 V is reported. These incorporate a novel triazolobenzothiadiazole-based emitter and a novel indacenodithiophene-based transport polymer matrix, affording excellent spectral and transport properties. To the best of knowledge, such values are the best ever reported for electroluminescence at 840 nm with a purely organic and solution-processed active layer, not leveraging triplet-assisted emission.

Dr. A. Minotto, Dr. A. Zampetti, G. Carnicella, Prof. F. Cacialli
Department Physics and Astronomy and London Centre for
Nanotechnology
University College London
London WC1H 0AH, UK
E-mail: f.cacialli@ucl.ac.uk
P. Murto, Dr. Z. Genene, Prof. E. Wang
Department of Chemistry and Chemical Engineering/Applied Chemistry
Chalmers University of Technology
Gothenburg SE-412 96, Sweden
E-mail: ergang@chalmers.se
Dr. Z. Genene, Prof. W. Mammo
Department of Chemistry
Addis Ababa University
Addis Ababa, P.O. Box 33658, Ethiopia
P. Murto, Prof. M. R. Andersson
Flinders Institute for NanoScale Science & Technology
Flinders University
Sturt Road, Bedford Park, Adelaide, SA 5042, Australia

(iD) The ORCID identification number(s) for the author(s) of this article can be found under https://doi.org/10.1002/adma.201706584.

The development of efficient and biocompatible organic near-infrared emitters is attractive for many applications, spanning from photodynamic therapy[1] to light fidelity (Li-Fi) all-optical networking systems.[2–4] In particular, the range 700–1000 nm is interesting for medical applications, given the semitransparency of biological tissue in this spectral interval,[5] and we will specifically refer to this range as near-infrared (NIR) in the following text. Compared to conventional inorganic materials, organic NIR emitters are interesting also for their mechanical conformability, which makes them appealing for the integration in flexible and stretchable devices.[6] Furthermore, the metal-free organic light-emitting materials can be a cheap and biocompatible alternative to inorganic ones for application in wearable, implantable, or in vivo medical applications, such as for sensing of body temperature, heart and respiration rates, blood pressure, glucose level, and oxygenation.[7]

In the search for ever-higher efficiencies, several classes of materials have been investigated, such as perovskite-structured methylammonium lead halides,[8–10] quantum dots,[11] and organometallic phosphorescent complexes.[12–19] However, although such hybrid materials afford substantial electroluminescence (EL) external quantum efficiency (EQE) in the NIR, in some cases exceeding 10%[8,10] or even 20% or so,[13] their use of heavy, toxic, and/or costly metals is not ideal for manufacturing, sustainability, environmental impact, and, in perspective, biocompatibility. Furthermore, in such hybrid systems, and in general in materials that leverage triplet excitons to boost the EQE,[20,21] exciton recombination dynamics typically fall in the hundreds of nanoseconds or even in the microsecond (or longer) range, which intrinsically limits the bandwidth when integrated in devices for telecommunications. For Li-Fi applications,[2–4] fluorescent molecular and polymeric materials are preferred, given that the typical fluorescence lifetime of these materials is of the order of few nanoseconds or less, thereby ideally allowing data transmission rates up to the Gb s⁻¹ regime.

In the last decade, scientists have attempted different strategies to develop heavy-metal-free NIR fluorescent organic light-emitting diodes (OLEDs), with chemical design essentially revolving around the careful combination of donor and acceptor groups to both tune the spectral range (up to 1000 nm) and maximize the EQE.[22–33] Very recently, we have, for

example, reported an acceptor–donor–acceptor (A–D–A) dye, which, embedded in a polyfluorene matrix, yielded EL peaked at 720 nm with 1.1% maximum EQE,[34] the best result ever reported in this range, to the best of our knowledge, for materials with intrinsic lifetimes <10 ns, thus suitable for "visible" (or nearly visible) light communication (VLC) systems.

Although such values might appear low, if compared with those of "fully" visible emitters (400–700 nm), we emphasize that this is in fact expected because of the so-called "energy-gap law,"[35] stating that for chemically similar chromophores, the fluorophore nonradiative rate increases exponentially as the energy gap is reduced. Furthermore, we note that to achieve NIR emission, one needs systems with extended planarity that can benefit from a concomitant extended conjugation, thereby leading to an even higher tendency to form cofacial (H-type) aggregates compared to visible emitters. To counteract the latter, NIR chromophores can be diluted in solid-state matrices,[34,36,37] which however have to be carefully chosen to prevent phase separation, and ensure maximum solubility, so that the majority of the emitters are physically isolated and, at the same time, afford efficient and optimum charge transport through the matrix. A possible strategy to reduce phase separation is to copolymerize the NIR moiety with a polymer host with a wider bandgap,[29,30] so as to restrict the chances of the chromophores to aggregate freely. For example, we recently reported NIR OLEDs incorporating as metal-free emitter a triazolobenzothiadiazole (BTT) moiety copolymerized with a wider-gap polymeric host (poly[3,3′-ditetradecyl-2,2′-bithiophene-5,5′-diyl-*alt*-5-(2-ethylhexyl)-4*H*-thieno[3,4-*c*]pyrrole-4,6(5*H*)-dione-1,3-diyl] (P2T-TPD)),[30] exhibiting EL peaked at 900 nm, albeit with maximum EQE of ≈0.15%.

Even though copolymerization of the emitter and host matrix might appear to be a superior approach when compared to blending, especially in terms of phase separation, we note that: i) chromophore aggregation or close packing is still possible in copolymers (i.e., due to either interchain interactions, as also in blends, or even due to intrachain interactions in the presence of hairpin or similar defects). For random copolymers, it is also hard to control the distribution of the different moieties in the polymer backbone, and confirm the exact amount incorporated in the copolymers; ii) it is very difficult to study the evolution of the frontier levels of each moiety upon copolymerization, thereby potentially affecting the intended heterojunction design, which might end up not being type-I, which is preferred to favor energy transfer over charge transfer (see **Figure 1** and Figure S22 (Supporting Information)); and iii) combination of different dyes with suitable host matrices by copolymerization is significantly more costly than a blend-based approach.[38] In fact, blending can offer an alternative strategy for combining different desirable properties, and thus afford "the best of all worlds."[38] Clearly, the host matrices still need to be selected carefully so as to allow type-I heterojunctions with the dye, as well as to ensure good spectral overlap between the host photoluminescence and the guest absorption. Interestingly, poly(9,9′-dioctylfluorene-*alt*-benzothiadiazole) (F8BT) has often been found to behave as the best host polymer in previous NIR OLED reports, in spite of relatively poor spectral overlaps, likely as a result of its excellent electron transport and triplet-assisted emission properties (the "F8BT paradox").[34,36,37]

Here, we propose a novel blend featuring a modified BTT emitter (BTT*, Figure 1a), and a novel red/NIR polymeric host (PIDT-2TPD), intentionally designed for charge transport and spectral overlap that allow unprecedented performance in terms of EQEs and turn-on voltage (V_{ON}) in the spectral range above 800 nm.

The NIR dye (BTT*) is engineered to incorporate a central BTT unit in between bithiophenes that act as the donors of a D–A–D structure. This is complementary to the recently reported A–D–A motif of NIR-emitting 4,4-difluoro-4-bora-3a,4a-diaza-*s*-indacene (BODIPY) units.[34]

For the host matrix we also opted for an alternating D–A structure, as the indacenodithiophene (IDT) moiety (pale-blue shading in Figure 1b,c) behaves as a donor, and the thieno[3,4-*c*]pyrrole-4,6-dione (TPD) moiety (pale red in Figure 1b) behaves as an acceptor. However, PIDT-2TPD (Figure 1c), presented here for the first time, benefits from the presence of two interconnected acceptor units (bithieno[3,4-*c*]pyrrole-4,4′,6,6′-tetrone or 2TPD), instead of just one, as in PIDT-TPD[39] (also shown in Figure 1b, and also used as a control) and a subsequently stronger acceptor nature, expected to improve electron transport. In addition, both hosts form a type-I heterojunction with BTT* (Figure 1e,f) and feature excellent spectral overlaps of their photoluminescence with the BTT* absorption.

Remarkably, we obtained the best results from OLEDs based on blends of BTT* with the novel PIDT-2TPD matrix: virtually (98%) pure NIR EL peaked at 840 nm with a turn-on voltage (V_{ON}) of only 1.7 V, EQE in excess 1.15%, and 1.5 mW cm^{-2} optical output. To the best of our knowledge, such values are the best ever reported in this spectral range from a polymer-based light-emitting diode (PLED) based on a heavy-metal-free, solution-processed active layer not "intentionally" leveraging triplet-assisted emission (e.g., as for thermally activated delayed fluorescence materials).[21]

To obtain the BTT* NIR emitter, we re-engineered a previously reported BTT-based monomer featuring just one thiophene unit on either side of BTT,[30] by introducing an additional thiophene on either side of the molecule (Figure 1a and Figure S1 (Supporting Information)), so as to decrease the energy gap and thus further redshift the emission of the dye into the NIR region. In addition, to obtain good miscibility with the host polymer matrices and improve the solubility in organic solvents, such as toluene used in this study, we specifically tailored branched 2-butyloctyl side chains in both the BTT-based acceptor and the thiophene donors.

We synthesized PIDT-TPD and PIDT-2TPD polymers by copolymerization via Pd-catalyzed Stille coupling of bis(trimethylstannyl)-substituted IDT and 1,3-dibromo-TPD or 3,3′-dibromo-2TPD monomers, respectively (Figure S3, Supporting Information). 2TPD has been prepared via a six-step synthesis route, starting from a Gewald-type condensation between methyl pyruvate, ethyl 2-cyanoacetate, and sulfur to obtain the heterocyclic core structure,[40,41] as described in the Experimental Section and Figure S2 (Supporting Information). The polymers were end-capped and purified to remove any Pd or Sn residues,[42–44] as described in detail in the Supporting Information. We used 2-octyldodecyl side chains on 2TPD to increase the solubility of the resulting polymer and also provide satisfactory steric hindrance to prevent aggregation.[41,45] Likewise, even though IDT-based copolymers in general show low degree of long-range ordering in the solid state compared to semicrystalline
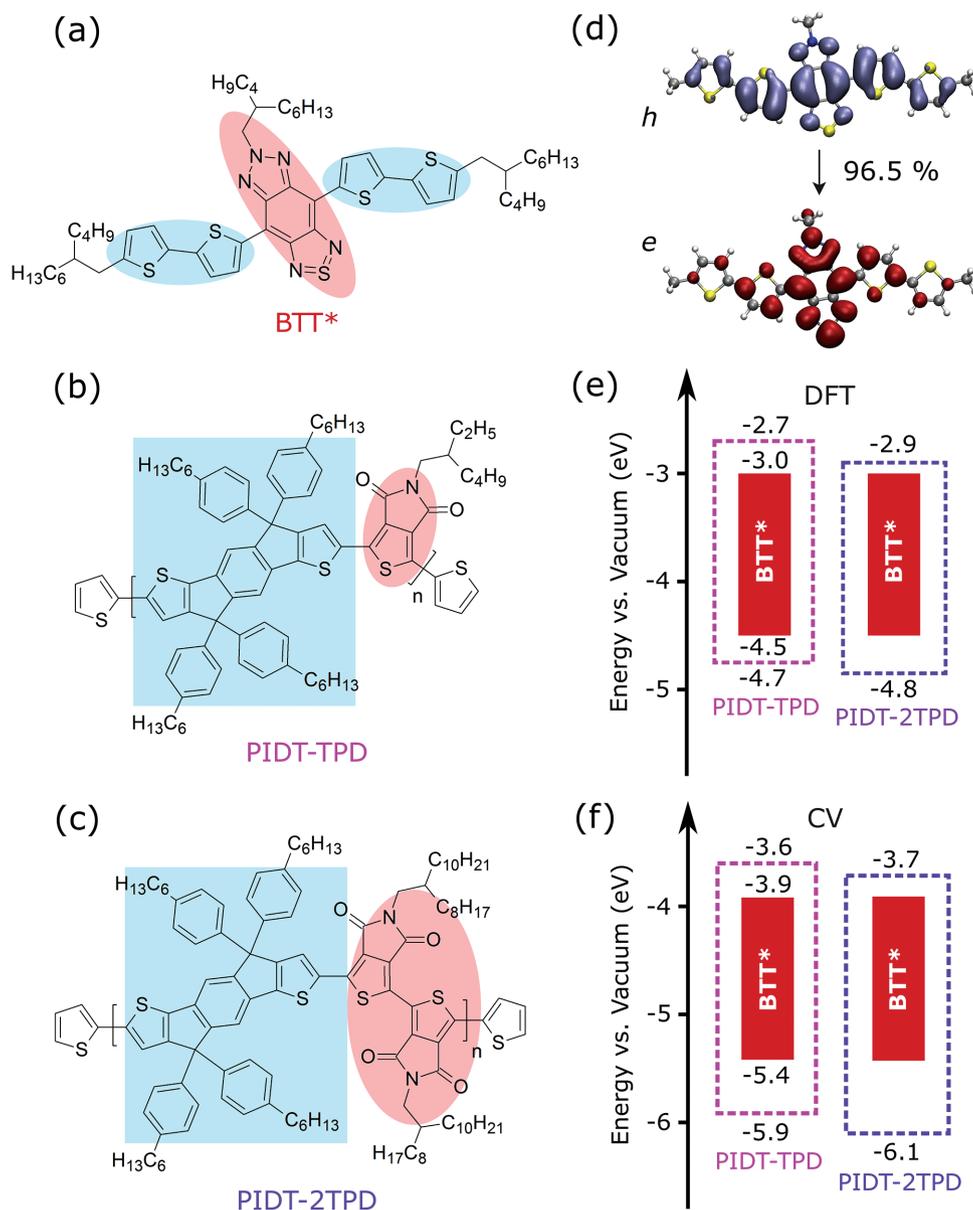
Figure 1. a–c) Molecular structures of the BTT* NIR dye and PIDT-TPD/PIDT-2TPD host polymers. Pale blue and red shadings highlight the electron donor and acceptor units, respectively. The extended International Union of Pure and Applied Chemistry (IUPAC) molecular denominations are reported in the Supporting Information. d) Natural transition orbital analysis (h = hole, e = electron) of the lowest excited singlet state (S$_1$) for the BTT* model compound, as calculated at ωB97XD*/6-31G(d,p) level. The percentage stands for the contribution of such orbitals to the transition. e) HOMO and LUMO energy levels calculated at B3LYP/6-31G(d,p) level. Dashed boxes schematically represent the bandgaps of the host matrices, whereas the red boxes stand for the BTT* gap. f) HOMO and LUMO energy levels measured by cyclic voltammetry. Both DFT and CV show that the energy gap of BTT* is contained in the one of both polymer hosts to form a type-I heterojunction.

polymers,[46–48] we functionalized the planar IDT backbone with bulky *p*-hexylphenyl substituents (Figure 1b,c), which are expected to further reduce polymer chain aggregations as they align somewhat perpendicular to the planar IDT backbone.[49,50] We obtained higher number-average molecular weight (M_n) for PIDT-2TPD (55.7 kg mol^{-1}, polydispersity index (PDI) 2.4) due to the much longer side chains attached on 2TPD as compared to PIDT-TPD (26.3 kg mol^{-1}, PDI 2.1), yet comparable PDIs.

Thermogravimetric analysis (Figure S4, Supporting Information) revealed that both the PIDT-TPD and PIDT-2TPD host

copolymers and BTT* molecule exhibit high thermal stability with no significant weight loss until 400 °C. For the polymers, no detectable thermal transition is observed on differential scanning calorimetry (DSC) measurements in the range 25–325 °C (Figure S5, Supporting Information). The DSC scan for BTT* (in the range −75–225 °C) reveals two distinctive phase transitions upon heating, which correspond to exothermic crystallization (T_c) at −1 °C and endothermic melting (T_m) of the crystallized phase at 87 °C (Figure S6, Supporting Information). These transitions are not observed in the blends with PIDT-TPD and PIDT-2TPD

host copolymers, as shown in Figure S6 (Supporting Information).

To study the electronic properties of the NIR dye and of the host copolymers, we carried out both density functional theory (DFT) calculations and cyclic voltammetry (CV) measurements. The detailed methodology of the DFT calculations and CV measurements are reported in Figures S7–S19 (Supporting Information) and the Experimental Section.

In Figure 1d, we show the calculated hole and electron spatial distribution of the BTT* molecule with the optimized lowest excited singlet state (S_1) geometry. We observe that the hole is well distributed along the BTT* molecular backbone, whereas the electron is more localized on the BTT (core) electron acceptor. Although the offsets between the highest occupied molecular orbital (HOMO) and lowest unoccupied molecular orbital (LUMO) energy levels of the bithiophene and BTT segments further confirm their relatively strong electron-donor and electron-acceptor nature, respectively (Figure S18, Supporting Information), the hole and electron of BTT* show partial overlap at the S_1 state similarly to the HOMO and LUMO in its ground state (Figure S17, Supporting Information). This suggests that BTT* exhibits a local excited (LE) state character, with electron localization around the core of the molecule (BTT), good spatial overlap with the hole wavefunction, and a concomitantly large singlet exciton yield.[51–55] Notably, the resulting exciton is thus expected to be preferentially localized on the center of the NIR emitting dye, and thereby be somewhat protected from quenching defects and impurities in the blend.

The calculated HOMO and LUMO energy levels of the PIDT-TPD and PIDT-2TPD host copolymers and the BTT* molecule are shown in Figure 1e. However, two caveats must be taken into account: first, the essentially complete delocalization of the frontier orbitals might be due to the tendency of B3LYP functional to overestimate the energy barrier of rotational torsion and thus the planarity of the backbone,[56,57] and second, HOMO and LUMO charge distributions might be different in the solid-state compared the ideal gas-phase conditions of the DFT calculations (see the Supporting Information for further details). According to our calculations, however, by blending BTT* in the two different polymers, we should obtain bulk heterojunctions exhibiting a type-I bandgap alignment. Notably, this is fully supported by results from CV, as shown in Figure 1f, within minor numerical discrepancies typical of DFT calculations.

As shown in Figure S20 (Supporting Information), both PIDT-TPD and PIDT-2TPD exhibited relatively good electrochemical stability and quasireversible oxidation and reduction processes in our CV measurements. Compared to the BTT-based monomer previously reported,[30] in BTT*,
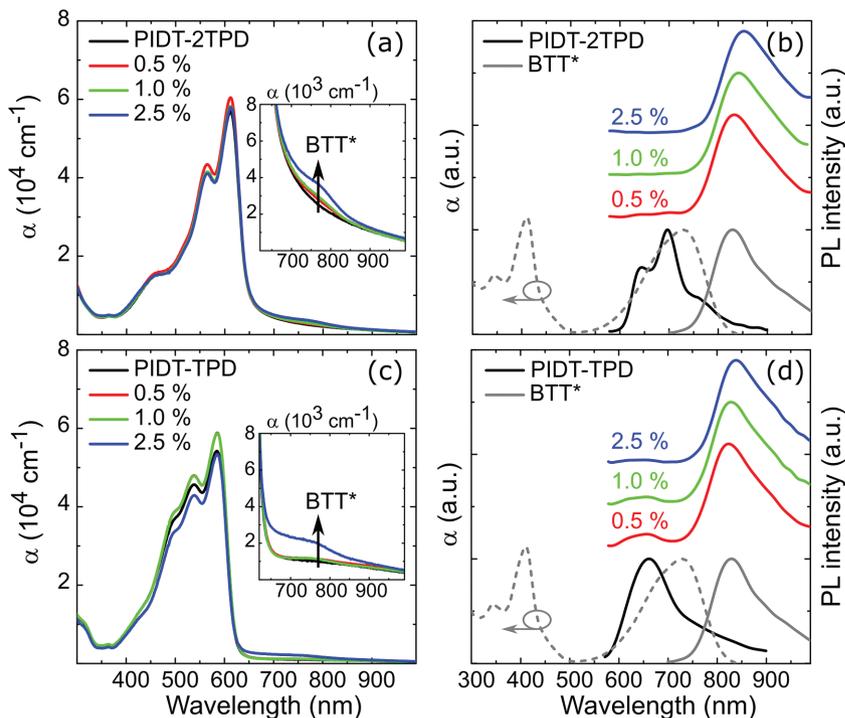

Figure 2. a,c) Absorption spectra of the host polymers and blends containing 0.5, 1, 2.5 wt% of BTT* in solid-state thin films (≈100 nm) spin-cast on fused silica substrates. The black arrow indicates the increasing BTT* absorption with increasing doping concentration. b,d) PL spectra measured in air and at room temperature by exciting the samples with a 520 nm laser diode, which is resonant with the absorption of both the hosts. Gray lines represent the absorption (dashed line) and photoluminescence of BTT* in a toluene solution. The PL from the BTT* toluene solution was measured by exciting the sample with a 670 nm laser diode. The solution was prepared in a 10 mm path quartz cuvette with an absorbance of <0.15 at the lowest energy absorption maximum, following a protocol reported in the literature.[57]

the HOMO and LUMO energy levels increase by 0.40 and 0.26 eV, respectively, corresponding also to a 0.14 eV reduction of the energy gap, as expected for the more extended conjugation of BTT*.

We report in **Figure 2** the absorption and photoluminescence (PL) spectra of BTT* in toluene solution and in solid-state blends with the PIDT-2TPD and PIDT-TPD host matrices. In particular, we characterized blends with 0.5, 1, and 2.5 wt% content of BTT*, whose photoluminescence quantum yields (PLQY) are reported in **Table 1**.

As it can be noted in Figure 2b,d (gray dashed line), BTT* in toluene solution exhibits two absorption bands: one in the blue, peaked at 410 nm, and the other in the red/NIR, with the maximum at 730 nm. By exciting the BTT* solution at 670 nm, we measured a purely NIR PL spectrum (Figure 2b,d, gray line) peaked at 830 nm with PLQY = 29 ± 3%, which is among the highest values reported so far for a metal-free NIR emitter.[58]

The absorption spectra of PIDT-2TPD and PIDT-TPD are peaked at 620 and 580 nm, respectively. As highlighted in the insets of Figure 2a,c, the absorption spectra of the respective blends with BTT* exhibit an increasing NIR absorption band at ≈750 nm, which corresponds to the lowest energy absorption band of the molecule (Figure 2b,d, gray dashed line).

As the PL spectra of PIDT-2TPD and PIDT-TPD are peaked at 700 and 660 nm (black line in Figure 2b,d) they both offer

Table 1. Photoluminescence quantum yield (PLQY) of the PIDT-2TPD and PIDT-TPD solid-state thin films ($\approx$100 nm, spin-cast on fused silica substrates) with different BTT* loadings. PLQY values were measured with an integrating sphere setup and a 520 nm laser diode (in air, at room temperature). Each PLQY value reported here is averaged over ten independent measurements, with a 10% standard deviation.

Sample	PLQY [%]	NIR fraction[a] [%]	Sample	PLQY [%]	NIR fraction[a] [%]
PIDT-2TPD	18	50	PIDT-TPD	5	25
0.5 wt% BTT*	17	95	0.5 wt% BTT*	18	95
1.0 wt% BTT*	19	99	1.0 wt% BTT*	16	99
2.5 wt% BTT*	11	99	2.5 wt% BTT*	12	99

[a]% of photons emitted at $\lambda > 700$ nm.

excellent spectral overlap with the BTT* absorption (and much better than for F8BT[34]). Remarkably, PIDT-2TPD exhibits PLQY = 18 ± 3%, which is comparatively high for this spectral range, considering that half of the photons are emitted in the NIR (Table 1). Both absorption and PL of PIDT-2TPD exhibit a better-defined vibronic structure with respect to PIDT-TPD, possibly as a result of a higher rigidity and reduced electronic disorder of the polymer chains in the solid state. Interestingly, we also show DSC scans in the range 25–325 °C, in Figure S5 (Supporting Information), which do not reveal features that could be associated with either melting or crystallization, although DSC is not very sensitive for the detection of crystallinity of conjugated polymers.

The spectral overlap between the BTT* absorption and the matrix polymers PL (Figure 2b,d), ensures that the fraction of photons emitted at $\lambda > 700$ nm (for both matrices) is $\approx$95% of the overall emission for blends with 0.5 wt% BTT*, and increases to 99% for blends with 1 and 2.5 wt% concentration of BTT* (Table 1). The resulting PL of the blends (resulting from BTT*) peaks at 830 nm, as for the BTT* toluene solutions. The PL spectrum further redshifts with concentration, due to increasing packing interactions in the solid-state matrix. Note however, that from transient PL measurements we carried out on the blends (Figure S21, Supporting Information), we extracted a single exponential decay with an $\approx$2.5 ns lifetime, providing clear evidence that the PL arises from a singlet exciton, albeit slightly longer-lived than for other organic semiconductors.[59]

As reported in Table 1, we are able to retain a solid-state PLQY > 15% by limiting the BTT* loading to ≤1% for both blends. To the best of our knowledge, such PLQY values are the highest reported so far for a metal-free moiety in the solid state and emitting in this spectral range.[21]

In this regard, we also note that although the PL quantum yield of a pure species only depends on the ratio of the radiative to the sum of the radiative and nonradiative decay constants (for monomolecular decay), the case is indeed more complicated in the case of a blend, and the factors influencing the PLQY of the acceptor when selectively exciting the matrix (donor) in the blends, depend on the interplay of the PLQY of both donor and acceptor, and on the efficiency of energy transfer, which also involve spectral overlap between the donor emission and acceptor absorption spectra. In our case, the PLQY of the isolated PIDT-2TPD is 18% but lower for PIDT-TPD (5%). Importantly, we can extract the radiative and nonradiative rates for the pure materials from analysis of the lifetimes (τ = 0.5 and 0.8 ns for PIDT-2TPD and PIDT-TPD, respectively, from

time-correlated single-photon counting, TCSPC, measurements) and PLQY for the pure materials as $k_r = \text{PLQY}/\tau$ and $k_{nr} = 1/\tau - k_r$. By approximating the PLQY of BTT* in the 0.5 wt% blend with that of its solution ($\eta_{\text{PLBTT*}} = 29\%$), we calculate an energy transfer efficiency ($\eta_{ET} = \eta_{\text{PLBTT*}}^{\text{Blend}}/\eta_{\text{PLBTT*}}$ where $\eta_{\text{PLBTT*}}^{\text{Blend}}$ is the PLQY of BTT* once incorporated in the blend) of $\approx$56% and $\approx$59% for PIDT-2TPD and PIDT-TPD, respectively, and an energy transfer rate $k_{ET} \approx 2.5 \times 10^9$ and 1.8×10^9 s^{-1} for PIDT-2TPD and PIDT-TPD, respectively. Thanks to this relatively high transfer rate (compared to the nonradiative rate k_{nr}, we find $k_{ET}/k_{nr} \approx 1.5$ in both cases) that the NIR PLQY of both blends is very similar ($\approx$16% and $\approx$17% for PIDT-2TPD and PIDT-TPD, respectively) despite the very different PLQYs of the pure hosts. This is because the energy transfer process competes in a comparably effective manner with the nonradiative processes in both blends, essentially regardless of the (significantly) different k_r values in the two host polymers (0.36×10^9 and 0.062×10^9 s^{-1} for PIDT-2TPD and PIDT-TPD, respectively).

Building on the powerful insight provided by the above results, we fabricated solution-processed undoped PLEDs incorporating either PIDT-2TPD or PIDT-TPD, as well as PLEDs having 0.5, 1, and 2.5% blends with BTT* as NIR emitting layer. For all devices, we used indium tin oxide/poly(3,4-ethylene dioxythiophene) doped with poly(styrene sulfonate) (ITO/PEDOT:PSS) anodes and Ca/Al cathodes.[34] The PLEDs' most significant parameters are summarized in **Table 2**, whereas typical EL spectra, current density/radiance versus bias voltage (JVR) plots and EQE versus current density plots for the neat polymers and the best performing 0.5% blends are illustrated in **Figure 3**. The EL spectra measured at different voltage bias

Table 2. Summary of the most relevant PLED characteristics.

Sample	V_{ON} [V]	$\langle R_{\text{MAX}}\rangle$ [mW cm^{-2}]	$\langle EQE_{\text{MAX}}\rangle$ [%]	EL in NIR[a] [%]
PIDT-2TPD	1.7 ± 0.1	2.3 ± 0.5	1.55 ± 0.10	46
0.5 wt% BTT*	1.7 ± 0.1	1.5 ± 0.4	1.09 ± 0.05	98
1.0 wt% BTT*	1.7 ± 0.1	1.3 ± 0.3	0.88 ± 0.04	98
2.5 wt% BTT	1.7 ± 0.1	0.3 ± 0.1	0.87 ± 0.06	99
PIDT-TPD	1.9 ± 0.1	0.9 ± 0.2	0.36 ± 0.02	34
0.5 wt% BTT*	2.0 ± 0.2	1.4 ± 0.3	0.48 ± 0.01	94
1.0 wt% BTT*	1.8 ± 0.1	1.7 ± 0.3	0.43 ± 0.03	96
2.5 wt% BTT	2.3 ± 0.2	0.3 ± 0.1.	0.31 ± 0.11	96

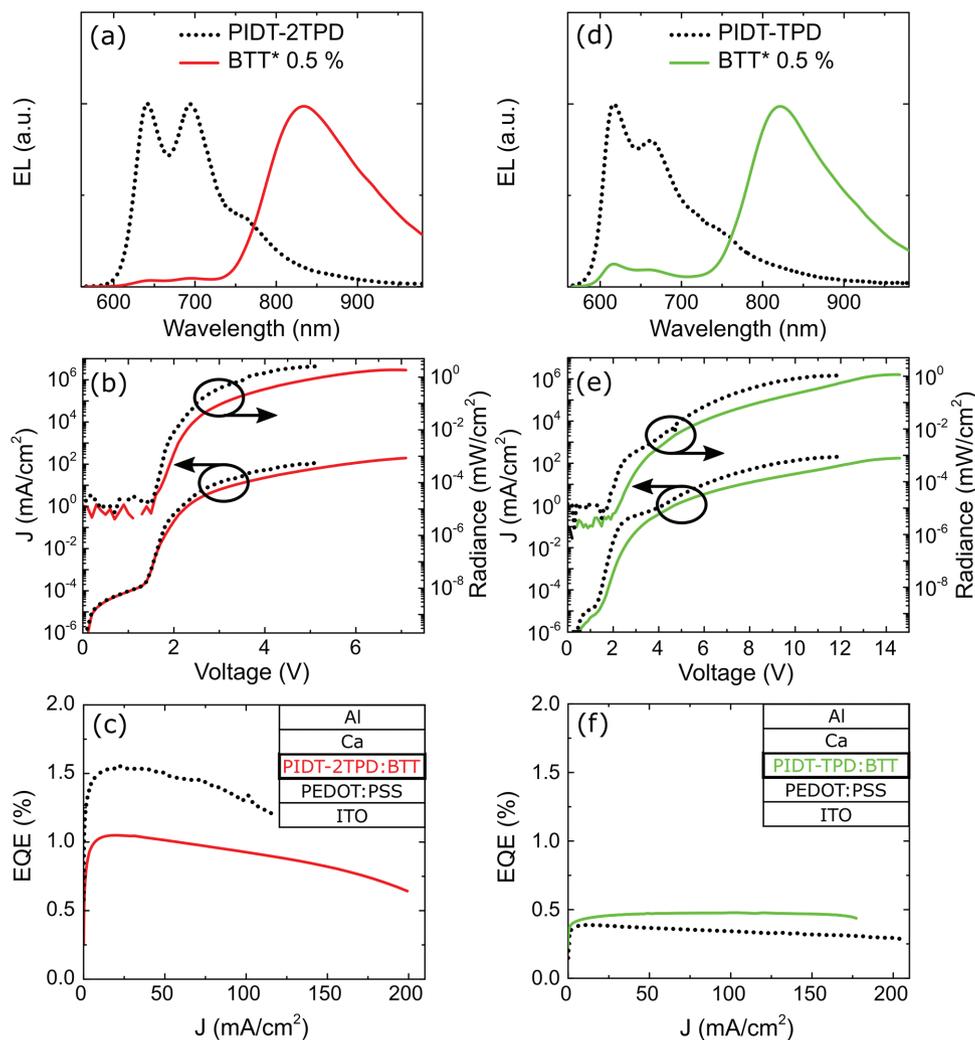[a]% of photons emitted at $\lambda > 700$ nm.

Figure 3. Characteristics of PLEDs incorporating PIDT-2TPD, PIDT-TPD, and blends with 0.5 wt% of BTT*. a,d) EL spectra, b,e) *JVR*, and c,f) EQE versus current density plots. The architecture of the devices is schematically illustrated in the insets. The EL spectra were measured at 4 V (PIDT-2TPD devices) and 10 V (PIDT-TPD devices).

and the *JVR*/EQE plots of 1% and 2.5% blends are reported in Figures S23 and S24 (Supporting Information), respectively.

Looking first at the PLEDs incorporating the neat polymers, we note that both the "pure" PIDT-2TPD and PIDT-TPD host polymers exhibit red/NIR EL, with, respectively, ≈1/2 and ≈1/3 of photons emitted at $\lambda > 700$ nm (NIR) (Figure 3a,d and Table 2), thereby confirming that both such matrices are better than F8BT (regarding spectral overlap), but with the matrix containing the interconnected 2TPD yielding even better spectral overlap with BTT*. The vibronic structure of the PIDT-2TPD EL spectrum resembles the one of the PL (Figure 2b), although the intensity of the 0–0 vibronic component peaked at 640 nm increases with respect to the 0–1 at 695 nm. A similar behavior is observed in the case of PIDT-TPD, for which the vibronic structure of the EL spectrum is much better defined compared to the PL (Figure 2d). Both the redistribution of the intensity of the different vibronic lines and the slight blueshift of the EL with respect to the PL might be due to either optical interference effects induced by the metal cathode reflector,[60] or to

thermochromism, i.e., thermally activated decrease of the oligomer chain planarity as an electric current is applied (and the temperature slightly raised).[61]

Interestingly, the luminance turn-on voltage is as low as 1.6 V for PIDT-2TPD (Figure 3b and Table 2), i.e., nominally corresponding to a NIR emission wavelength of ≈775 nm, thus powerfully confirming that the addition of an extra TPD group affords optimum charge injection and transport properties, also compared to PIDT-TPD, for which we observe a slightly higher turn-on voltage of 1.9 ± 0.1 V (Figure 3e and Table 2). Furthermore, we recorded average maximum radiances of 2.3 mW cm^{-2} from PLEDs based on PIDT-2TPD (Table 2). The latter exhibits also one of the highest EQE (≈1.5%, Table 2) reported so far in the literature for a red/ NIR emitting metal-free polymer.[21] Notably, the maximum EL efficiency of PIDT-2TPD (see Figure 3c) was measured at a relatively low driving voltage (≈3.5 V) and at a current density of ≈20 mA cm^{-2}, which corresponds to an optical output of ≈0.5 mW cm^{-2}.

To get further insight into the transport properties of the polymeric host materials, we also fabricated hole-only and electron-only devices, whose current density versus voltage (JV) characteristics are discussed fully in Figure S25 and the related discussion (Supporting Information). For (bipolar) PIDT-2TPD PLEDs, such data reveal that the total current density is dominated by the space-charge limited hole current ($\propto V^2$) below the radiance turn-on (≈ 1.7 V), with a mobility of $\approx 3 \times 10^{-5}$ cm^2 V^{-1} s^{-1}, and that the electron current (consistent with a trap-filled transport mechanism and $\propto V^{r+1}$ with $r = 2.5$) prevails for an applied bias exceeding the built-in voltage (V_{BI}) by at least 0.5 V. For PIDT-TPD devices instead, the current is always electron-dominated for ($V - V_{BI}$) > 0.1. Interestingly, neither PIDT-2TPD nor PIDT-TPD exhibits a trap-limited electron current (even in the lowest voltage range explored here), as if all the trap states (if any are present) were filled already at low voltage. Remarkably, the current of electron-only PIDT-2TPD devices displays a much steeper voltage dependence compared to PIDT-TPD ones, thereby suggesting a different average energetic trap depth and distribution in the different polymers.[62]

Turning now to the blends, we observe that PIDT-2TPD PLEDs containing 0.5 wt% of BTT* gave the best results in the NIR. Such PLEDs exhibited EL emission ($\approx 98\%$ in the NIR region) peaked at 840 nm (Figure 3a and Table 2), average maximum radiance of 1.55 mW cm^{-2}, turn-on voltage of 1.7 V, and EQE up to 1.16% ($1.09 \pm 0.05\%$ on average). Furthermore, such PLEDs could be operated up to 200 mA cm^{-2} while maintaining the EQE above 0.5% (Figure 3c and Table 2). By considering the PLQY = 17% of the 0.5 wt% blend (Table 1) and the 1.73 refractive index of PIDT-2TPD at 830 nm (obtained via ellipsometry, Figure S28, Supporting Information), in the ideal case of unit charge injection efficiency, we expect EQEs ranging from 0.78% to 1.87% (depending on the orientation of the emitting dipoles and their location with respect to the metal cathode reflector),[63] thereby confirming that there are only very minor improvements that can be expected upon further optimization of the device architecture.

In terms of NIR purity of the emission, thanks to efficient energy and charge transfer, the EL component from PIDT-2TPD is almost completely quenched by BTT* (Figure 3a,d). As for the neat PIDT-2TPD polymer, the blend devices exhibit well-behaving JVR characteristics (Figure 3b). Namely, up to ≈ 1.7 V, the diodes behave as unipolar hole-only devices as expected, given the relatively high hole mobility in indacenodithiophene-based copolymers.[64] Beyond such threshold, electron transport is also activated and light is emitted. Remarkably, the average radiative turn-on voltage for the blend devices is essentially the same (within experimental scatter of 0.1 V) as that observed for the pure PIDT-2TPD PLEDs, thereby confirming that most charge injection/transport occurs via the matrix. Note thus the advantage ensuing from the optimization of the polymer matrix here reported, also in terms of spectral overlap and driving conditions (and eventually dissipated power and operational stability), e.g., compared to other state-of-the-art devices.[13,20,34]

Overall, PIDT-TPD devices exhibit less efficient quenching of the host emission (via energy transfer), slightly higher turn-on voltages, less ideal JVR characteristics, and significantly lower EQEs (Table 2 and Figure 3d–f) compared to PIDT-2TPD-based ones. For such devices as well, the final performance in the NIR is influenced by the transport matrix, but the EQE never exceeds 0.5%, even though (differently from the PIDT-2TPD ones) it improves slightly upon addition of BTT*. We consider that such a different behavior is mainly due to the relatively low PLQY ($\approx 5\%$, Table 1) of the PIDT-TPD matrix (less than a third of that of PIDT-2TPD), which in turn indicates a higher density of nonradiative recombination centers/traps for charges and excitons in PIDT-TPD compared to the PIDT-2TPD. Incidentally, atomic force microscopy (AFM) imaging (Figures S26 and S27, Supporting Information) seems to suggest an evolution of the morphology in the sense of increasing roughness at increasing BTT* concentration (Figure S27, Supporting Information) in the PIDT-TPD blends, which we do not appear to observe with the best performing PIDT-2TPD ones (Figure S26, Supporting Information). However, although this might suggest a higher degree of phase separation in the PIDT-TPD blends and potential concomitant effects in terms of device performance, we consider that these effects are not substantial enough to enable us to confidently draw further conclusions in this regard, and therefore refrain from reading further correlation into this observation.

In conclusion, we report 840 nm emitting OLEDs with EQEs in excess of 1.15%. This has been achieved by engineering a novel polymer electroluminescent blend sporting a purpose-developed matrix (PIDT-2TPD) that has been mixed with a very-high efficiency novel triazolobenzothiadiazole-based emitter (BTT* with $\approx 30\%$ PLQY). PIDT-2TPD exhibits significantly improved characteristics compared to previously reported matrices, including F8BT, which had so far been the best host matrix for a large number of NIR OLEDs, despite its PL poor spectral overlap with the emitter absorption. To the best of our knowledge, the EQE and radiance we obtained from such a blend are the highest obtained so far from a fluorescent NIR OLED with EL peaked above 800 nm, and, crucially, within the class of devices based on an active layer free from heavy/toxic metals.[21] These results, together with the possibility to operate such devices up to 200 mA cm^{-2} while maintaining the EQE above 0.5% and turn-on voltages as low as 1.7 V make them promising candidates for application in wearable, skin-mounted, or implantable bioelectronics, in which an active layer free from heavy metals is of crucial importance.

Experimental Section

NIR Dye and Polymer Characterization: ^{1}H-NMR (400 MHz) and ^{13}C-NMR (100 MHz) spectra were recorded on an automated Varian Inova 400 MHz NMR spectrometer. Chemical shifts were given in δ (ppm) relative to the tetramethylsilane (TMS) peak at 0 ppm. CDCl$_3$ (^{1}H: 7.26 ppm; ^{13}C: 77.16 ppm), acetone-D$_6$ (^{1}H: 2.05 ppm; ^{13}C: 29.84, 206.26 ppm), and carbon disulfide (CS$_2$, ^{13}C: 193.58 ppm in acetone-D$_6$) were used as solvent.[65,66] Matrix-assisted laser desorption ionisation–time-of-flight (MALDI-TOF) spectra were recorded on a Bruker Daltonics Autoflex MALDI-TOF Mass Spectrometer. Size exclusion chromatography (SEC) was carried out for the copolymers on an Agilent PL-GPC 220 Integrated High Temperature GPC/SEC System with refractive index and viscometer detectors and three sequential PLgel 10 µm MIXED-B LS 300 × 7.5 mm columns. The eluent was 1,2,4-trichlorobenzene and the operating temperature was 150 °C. The molecular weights were calculated relative to calibration with polystyrene standards. Thermogravimetric analysis (TGA) was carried out using

Mettler Toledo TGA/DSC 3+ STAR System instrument, under nitrogen atmosphere over a temperature range of 30–550 °C and with a heating rate of 10 °C min^{-1}. The T_{onset} (corresponding to 1% weight loss) and T_{d95} were reported. DSC measurements were carried out on a Mettler Toledo DSC 2 STAR System instrument under nitrogen atmosphere, over a temperature range of 0–350 °C using a heating/cooling rate of 10 °C min^{-1} (for PIDT-TPD and PIDT-2TPD) and −100–250 °C using a heating/cooling rate of 5 °C min^{-1} (for BTT*, PIDT-TPD:BTT*, and PIDT-2TPD:BTT* blends). The graphs from the 2nd scan were reported.

Cyclic Voltammetry: CV measurements were done on a CH-Instruments 650A Electrochemical Workstation in a three-electrode cell using Pt wires as both the working electrode and the counter electrode, and Ag wire in 0.1 M AgNO$_3$ (MeCN/H$_2$O) as the reference electrode calibrated to ferrocene/ferrocenium (Fc/Fc$^+$) redox couple. A 0.1 M solution of tetrabutylammonium hexafluorophosphate (Bu$_4$NPF$_6$) in anhydrous acetonitrile was used as the electrolyte, which was bubbled with nitrogen prior to each measurement. The polymer films were deposited onto the working electrode from toluene solution. The oxidation and reduction were measured separately at a scan rate of 100 mV s^{-1}, with a minimum of four measurements for each film. The HOMO and LUMO levels were derived from the first oxidation and reduction onset potential (E_{ox} and E_{red}) by setting the Fc/Fc$^+$ oxidation onset potential versus the normal hydrogen electrode (NHE) to 0.630 V and the NHE to −4.5 V in the Fermi vacuum scale,[67–69] which gives the formula HOMO = −(E_{ox} + 5.13) eV and LUMO = −(E_{red} + 5.13) eV. The reversibility of the electrochemical oxidation and reduction processes was estimated from the separation of their cathodic (E_p^c) and anodic peak potentials (E_p^a), as $\Delta E_p = E_p^c − E_p^a$.

PL Characterization: Thin films were spin-casted onto fused silica substrates from 10 mg mL^{-1} toluene solutions. The films were deposited in a N$_2$ environment via spin-coating at 1500 rpm to obtain a thickness ≈ 100 nm, measured with a Dektak profilometer. Photoluminescence was collected from an Andor Shamrock 163 spectrograph coupled with an Andor Newton electron-multiplying charge-coupled device (EMCCD). The PLQY experiments were conducted using an integrating sphere setup, and by comparing the number of photons re-emitted to the number of photons absorbed. For the PLQY of BTT* in toluene, a dilute solution with an absorbance of <0.15 at the lowest energy absorption maximum was prepared. The solution was prepared in a 10 mm optical path length quartz cell, following a protocol reported in the literature.[70] Time-resolved PL measurements were carried out with a TCSPC spectrometer previously reported.[59]

PLED Characterization: ITO substrates were cleaned with acetone and isopropanol in an ultrasonic bath and treated in an O$_2$ plasma chamber for 10 min. A 40 nm layer of PEDOT:PSS (Sigma-Aldrich) was spin-coated at 5000 rpm from a 2.8 wt% dispersion in water and annealed at 150 °C for 10 min. The active layer was spin-coated on top of the annealed PEDOT:PSS from 10 mg mL^{-1} toluene solutions. A Ca/Al (30/200 nm) cathode was thermally evaporated on top. The samples were then characterized under an ≈10^{-2} mbar vacuum using a Keithley 2400 source meter for both the current measurement and the voltage supply. The optical output of the PLEDs was measured with a calibrated silicon photodiode and the EL spectra were collected with the same spectrometer employed for the PL experiments.

Supporting Information

Supporting Information is available from the Wiley Online Library or from the author.

Acknowledgements

Conflict of Interest

The authors declare no conflict of interest.

Keywords

[1] B. Jang, J. Park, C. Tung, I. Kim, Y. Choi, *ACS Nano* **2011**, *5*, 1086.
[2] D. Tsonev, S. Videv, H. Haas, *Proc. SPIE* **2014**, *9007*, 900702.
[3] P. A. Haigh, F. Bausi, Z. Ghassemlooy, I. Papakonstantinou, H. Le Minh, C. Flechon, F. Cacialli, *Opt. Express* **2014**, *22*, 2830.
[4] S. T. Le, T. Kanesan, F. Bausi, P. a. Haigh, S. Rajbhandari, Z. Ghassemlooy, I. Papakonstantinou, W. O. Popoola, A. Burton, H. Le Minh, F. Cacialli, A. D. Ellis, *Opt. Lett.* **2014**, *39*, 3876.
[5] A. M. Smith, M. C. Mancini, S. Nie, *Nat. Nanotechnol.* **2009**, *4*, 710.
[6] S. Choi, H. Lee, R. Ghaffari, T. Hyeon, D. H. Kim, *Adv. Mater.* **2016**, *28*, 4203.
[7] Y. Khan, A. E. Ostfeld, C. M. Lochner, A. Pierre, A. C. Arias, *Adv. Mater.* **2016**, *28*, 4373.
[8] N. Wang, L. Cheng, R. Ge, S. Zhang, Y. Miao, W. Zou, C. Yi, Y. Sun, Y. Cao, R. Yang, Y. Wei, Q. Guo, Y. Ke, M. Yu, Y. Jin, Y. Liu, Q. Ding, D. Di, L. Yang, G. Xing, H. Tian, C. Jin, F. Gao, R. H. Friend, J. Wang, W. Huang, *Nat. Photonics* **2016**, *10*, 699.
[9] X. Gong, Z. Yang, G. Walters, R. Comin, Z. Ning, E. Beauregard, V. Adinolfi, O. Voznyy, E. H. Sargent, *Nat. Photonics* **2016**, *10*, 253.
[10] Z. Xiao, R. A. Kerner, L. Zhao, N. L. Tran, K. M. Lee, T.-W. Koh, G. D. Scholes, B. P. Rand, *Nat. Photonics* **2017**, *11*, 108.
[11] G. J. Supran, K. W. Song, G. W. Hwang, R. E. Correa, J. Scherer, E. a. Dauler, Y. Shirasaki, M. G. Bawendi, V. Bulović, *Adv. Mater.* **2015**, *27*, 1437.
[12] K. R. Graham, Y. Yang, J. R. Sommer, A. H. Shelton, K. S. Schanze, J. Xue, J. R. Reynolds, *Chem. Mater.* **2011**, *23*, 5305.
[13] K. Tuong Ly, R.-W. Chen-Cheng, H.-W. Lin, Y.-J. Shiau, S.-H. Liu, P.-T. Chou, C.-S. Tsao, Y.-C. Huang, Y. Chi, *Nat. Photonics* **2017**, *11*, 63.
[14] L. Huang, C. D. Park, T. Fleetham, J. Li, *Appl. Phys. Lett.* **2016**, *109*, 233302.
[15] T. C. Lee, J. Y. Hung, Y. Chi, Y. M. Cheng, G. H. Lee, P. T. Chou, C. C. Chen, C. H. Chang, C. C. Wu, *Adv. Funct. Mater.* **2009**, *19*, 2639.
[16] J. R. Sommer, R. T. Farley, K. R. Graham, Y. Yang, J. R. Reynolds, J. Xue, K. S. Schanze, *ACS Appl. Mater. Interfaces* **2009**, *1*, 274.
[17] E. L. Williams, J. Li, G. E. Jabbour, *Appl. Phys. Lett.* **2006**, *89*, 83506.
[18] J. Xue, L. Xin, J. Hou, L. Duan, R. Wang, Y. Wei, J. Qiao, *Chem. Mater.* **2017**, *29*, 4775.

**ADVANCED
SCIENCE NEWS**

www.advancedsciencenews.com

**ADVANCED
MATERIALS**

www.advmat.de

[19] R. Tao, J. Qiao, G. Zhang, L. Duan, C. Chen, L. Wang, Y. Qiu, *J. Mater. Chem. C* **2013**, *1*, 6446.

[20] Y. Yuan, Y. Hu, Y.-X. Zhang, J.-D. Lin, Y.-K. Wang, Z.-Q. Jiang, L.-S. Liao, S.-T. Lee, *Adv. Funct. Mater.* **2017**, *27*, 1700986.

[21] D. H. Kim, A. D'Aléo, X. K. Chen, A. D. S. Sandanayaka, D. Yao, L. Zhao, T. Komino, E. Zaborova, G. Canard, Y. Tsuchiya, E. Choi, J. W. Wu, F. Fages, J. L. Brédas, J. C. Ribierre, C. Adachi, *Nat. Photonics* **2018**, *12*, 98.

[22] Q. Peng, A. Obolda, M. Zhang, F. Li, *Angew. Chem., Int. Ed.* **2015**, *54*, 7091.

[23] J. Xue, C. Li, L. Xin, L. Duan, J. Qiao, *Chem. Sci.* **2016**, *7*, 2888.

[24] L. Yao, S. Zhang, R. Wang, W. Li, F. Shen, B. Yang, *Angew. Chem., Int. Ed.* **2014**, *53*, 2119.

[25] S. Wang, X. Yan, Z. Cheng, H. Zhang, Y. Liu, Y. Wang, *Angew. Chem., Int. Ed.* **2015**, *130012*, 13068.

[26] T. T. Steckler, O. Fenwick, T. Lockwood, M. R. Andersson, F. Cacialli, *Macromol. Rapid Commun.* **2013**, *34*, 990.

[27] T. T. Steckler, M. J. Lee, Z. Chen, O. Fenwick, M. R. Andersson, F. Cacialli, H. Sirringhaus, *J. Mater. Chem. C* **2014**, *2*, 5133.

[28] D. M. E. Freeman, A. Minotto, W. Duffy, K. J. Fallon, I. McCulloch, F. Cacialli, H. Bronstein, *Polym. Chem.* **2016**, *7*, 722.

[29] G. Tregnago, T. T. Steckler, O. Fenwick, M. R. Andersson, F. Cacialli, *J. Mater. Chem. C* **2015**, *3*, 2792.

[30] P. Murto, A. Minotto, A. Zampetti, X. Xu, M. R. Andersson, F. Cacialli, E. Wang, *Adv. Opt. Mater.* **2016**, *4*, 2068.

[31] O. Fenwick, S. Fusco, T. N. Baig, F. Di Stasio, T. T. Steckler, P. Henriksson, C. Fléchon, M. R. Andersson, F. Cacialli, *APL Mater.* **2013**, *1*, 32108.

[32] F. Lombeck, D. Di, L. Yang, L. Meraldi, S. Athanasopoulos, D. Credgington, M. Sommer, R. H. Friend, *Macromolecules* **2016**, *49*, 9382.

[33] J. Xue, Q. Liang, Y. Zhang, R. Zhang, L. Duan, J. Qiao, *Adv. Funct. Mater.* **2017**, *27*, 1703283.

[34] A. Zampetti, A. Minotto, B. M. Squeo, V. G. Gregoriou, S. Allard, U. Scherf, C. L. Chochos, F. Cacialli, *Sci. Rep.* **2017**, *7*, 1611.

[35] R. Englman, J. Jortner, *Mol. Phys.* **1970**, *18*, 145.

[36] O. Fenwick, J. K. Sprafke, J. Binas, D. V Kondratuk, D. Stasio, H. L. Anderson, F. Cacialli, *Nano Lett.* **2011**, *11*, 2451.

[37] M. Sassi, N. Buccheri, M. Rooney, C. Botta, F. Bruni, U. Giovanella, S. Brovelli, L. Beverina, *Sci. Rep.* **2016**, *6*, 34096.

[38] F. Cacialli, M. Stoneham, *J. Phys.: Condens. Matter* **2002**, *14*, V9.

[39] C. L. Chochos, A. Katsouras, N. Gasparini, C. Koulogiannis, T. Ameri, C. J. Brabec, A. Avgeropoulos, *Macromol. Rapid Commun.* **2017**, *38*, 1600614.

[40] R. W. Sabnis, D. W. Rangnekar, N. D. Sonawane, *J. Heterocycl. Chem.* **1999**, *36*, 333.

[41] P. Berrouard, F. Grenier, J. R. Pouliot, E. Gagnon, C. Tessier, M. Leclerc, *Org. Lett.* **2011**, *13*, 38.

[42] J. K. Park, J. Jo, J. H. Seo, J. S. Moon, Y. D. Park, K. Lee, A. J. Heeger, G. C. Bazan, *Adv. Mater.* **2011**, *23*, 2430.

[43] S. Kim, J. K. Park, Y. D. Park, *RSC Adv.* **2014**, *4*, 39268.

[44] U. Koldemir, S. R. Puniredd, M. Wagner, S. Tongay, T. D. McCarley, G. D. Kamenov, K. Müllen, W. Pisula, J. R. Reynolds, *Macromolecules* **2015**, *48*, 6369.

[45] D. H. Lee, K. H. Kim, J. Shin, M. J. Cho, D. H. Choi, *J. Polym. Sci., Part A: Polym. Chem.* **2016**, *54*, 1228.

[46] X. Zhang, H. Bronstein, A. J. Kronemeijer, J. Smith, Y. Kim, R. J. Kline, L. J. Richter, T. D. Anthopoulos, H. Sirringhaus, K. Song, M. Heeney, W. Zhang, I. McCulloch, D. M. DeLongchamp, *Nat. Commun.* **2013**, *4*, 2238.

[47] D. Venkateshvaran, M. Nikolka, A. Sadhanala, V. Lemaur, M. Zelazny, M. Kepa, M. Hurhangee, A. J. Kronemeijer, V. Pecunia, I. Nasrallah, I. Romanov, K. Broch, I. McCulloch, D. Emin, Y. Olivier, J. Cornil, D. Beljonne, H. Sirringhaus, *Nature* **2014**, *515*, 384.

[48] J. S. Kim, J. H. Kim, W. Lee, H. Yu, H. J. Kim, I. Song, M. Shin, J. H. Oh, U. Jeong, T. S. Kim, B. J. Kim, *Macromolecules* **2015**, *48*, 4339.

[49] X. Xu, P. Cai, Y. Lu, N. S. Choon, J. Chen, B. S. Ong, X. Hu, *Macromol. Rapid Commun.* **2013**, *34*, 681.

[50] D. Dang, W. Chen, S. Himmelberger, Q. Tao, A. Lundin, R. Yang, W. Zhu, A. Salleo, C. Müller, E. Wang, *Adv. Energy Mater.* **2014**, *4*, 1.

[51] W. Li, Y. Pan, L. Yao, H. Liu, S. Zhang, C. Wang, F. Shen, P. Lu, B. Yang, Y. Ma, *Adv. Opt. Mater.* **2014**, *2*, 892.

[52] X. Han, Q. Bai, L. Yao, H. Liu, Y. Gao, J. Li, L. Liu, Y. Liu, X. Li, P. Lu, B. Yang, *Adv. Funct. Mater.* **2015**, *25*, 7521.

[53] T. Liu, L. Zhu, C. Zhong, G. Xie, S. Gong, J. Fang, D. Ma, C. Yang, *Adv. Funct. Mater.* **2017**, *27*, 1606384.

[54] C. Wang, X. L. Li, Y. Gao, L. Wang, S. Zhang, L. Zhao, P. Lu, B. Yang, S. J. Su, Y. Ma, *Adv. Opt. Mater.* **2017**, *5*, 1.

[55] H. Sun, Z. Hu, C. Zhong, X. Chen, Z. Sun, J.-L. Brédas, *J. Phys. Chem. Lett.* **2017**, *8*, 2393.

[56] J.-L. Brédas, *Chem. Mater.* **2017**, *29*, 477.

[57] S. Liu, Z. Kan, S. Thomas, F. Cruciani, J.-L. Brédas, P. M. Beaujuge, *Angew. Chem., Int. Ed.* **2016**, *55*, 12996.

[58] K. Rurack, M. Spieles, *Anal. Chem.* **2011**, *83*, 1232.

[59] A. Petrozza, S. Brovelli, J. J. Michels, H. L. Anderson, R. H. Friend, C. Silva, F. Cacialli, *Adv. Mater.* **2008**, *20*, 3218.

[60] F. Cacialli, S. E. Burns, H. Becker, *Opt. Mater.* **1998**, *9*, 168.

[61] G. Latini, A. Downes, O. Fenwick, A. Ambrosio, M. Allegrini, C. Daniel, C. Silva, P. G. Gucciardi, S. Patanè, R. Daik, W. J. Feast, F. Cacialli, *Appl. Phys. Lett.* **2005**, *86*, 9.

[62] H. T. Nicolai, M. M. Mandoc, P. W. M. Blom, *Phys. Rev. B: Condens. Matter Mater. Phys.* **2011**, *83*, 1.

[63] J.-S. Kim, P. K. H. Ho, N. C. Greenham, R. H. Friend, *J. Appl. Phys.* **2000**, *88*, 1073.

[64] W. Zhang, J. Smith, S. E. Watkins, R. Gysel, M. McGehee, A. Salleo, J. Kirkpatrick, S. Ashraf, T. Anthopoulos, M. Heeney, I. McCulloch, *J. Am. Chem. Soc.* **2010**, *132*, 11437.

[65] H. E. Gottlieb, V. Kotlyar, A. Nudelman, *J. Org. Chem.* **1997**, *62*, 7512.

[66] G. R. Fulmer, A. J. Miller, N. H. Sherden, H. E. Gottlieb, A. Nudelman, B. M. Stoltz, J. E. Bercaw, K. I. Goldberg, *Organometallics* **2010**, *29*, 2176.

[67] V. V. Pavlishchuk, A. W. Addison, *Inorg. Chim. Acta* **2000**, *298*, 97.

[68] A. J. Bard, L. R. Faulkner, *Electrochemical Methods: Fundamentals and Applications*, 2nd Ed., Wiley, New York **2001**.

[69] C. M. Cardona, W. Li, A. E. Kaifer, D. Stockdale, G. C. Bazan, *Adv. Mater.* **2011**, *23*, 2367.

[70] C. Würth, M. Grabolle, J. Pauli, M. Spieles, U. Resch-Genger, *Nat. Protoc.* **2013**, *8*, 1535.